Cardiac Microstructure Estimation from Multi-photon Confocal Microscopy Images

Babak Ghafaryasl[1,*], Bart H. Bijnens[1,3], Erwin van Vliet[2], Fátima Crispi[2], and Rubén Cárdenes[1,2]

[1] Physense, DTIC, Universitat Pompeu Fabra, Barcelona, Spain
[2] Fetal and Perinatal Medicine Research Group, IDIBAPS, Hospital Clinic de Barcelona, Spain
[3] ICREA, Barcelona, Spain
babak.ghafary@upf.edu

Abstract. Construction of realistic models of the muscle fibers in myocardium is relevant for simulating the electro-mechanical behavior of the heart. Advances in microscopy imaging have improved the potential for visualization of the 3D distribution of myocytes. In this paper, we propose an approach to identify cardiac fibers structures, in multi-photon confocal microscopy images. Our method is based on contrast invariant features such as the multi-scale local phase image, to obtain a tensor representation of the local structure. We show here some results obtained from multi-photon microscopy images acquired in a fetal rabbit heart, where the cardiac microstructure can be extracted from the image in terms of fiber direction as well as fiber compactness. Experiments from phantom data also show a successful application of the proposed methodology.

1 Introduction

The knowledge of the muscular (sub-) structure of the heart is essential for understanding the behavior of this organ, its motion, deformation and electrophysiological performance. The muscular cells, myocytes, are elongated cells that are arranged in a complex three-dimensional mesh. Nevertheless, some kind of linear alignment of these cells can be detected and the main direction can be identified at each position within the heart wall. This direction is known as the fiber direction, and it has been used to model and simulate the electromechanical properties of the heart [1–3]. In these studies, the assumption is that the electrical propagation travels preferentially along the fibers' direction.

Myocardial performance is also related to the cardiac fiber orientation so differences in the fiber structure can lead to an abnormal motion of the myocardium. Different studies includes the fiber orientation as a prior information for modeling the heart motion [4, 5]. These studies show that combining the information of fiber orientation with different imaging modalities can result in a more accurate motion model of heart.

* Corresponding author.

S. Ourselin, D. Rueckert, and N. Smith (Eds.): FIMH 2013, LNCS 7945, pp. 80–88, 2013.

Previous studies showed that the fiber orientation within myocardium determine the distribution of stress and fiber shortening during ejection period [6–9]. Small changes in the fiber orientation (10%) induce large variation (50%) of fiber stress [8]. Different statistical models of the cardiac fibers were presented previously [10, 11]. However none of these studies are accurate models of fiber direction in individual hearts to estimate local myofiber load. In this study we estimate the direction of fibers from microscopic information by detecting the direction of intracellular structures in the image. Our method consists of different stages to remove the illumination and noise artifacts using phase information of the image, identifying the local structures using a multi-scale feature extraction technique and finally visualization the fiber direction as streamlines. The performance of our method was tested by comparing angle fiber orientations extracted from our technique in a synthetic phantom with respect to their actual values.

2 Materials and Methods

2.1 Image Acquisition

For this study the images were taken from a normal fetal rabbit heart. The heart was fixed in 4% paraformaldehyde and was cut in half to fill the empty cavities. The tissue imaging was performed on a high speed multi-photon confocal microscope with integrated vibratome sectioning (TissueCyte 1000, TissueVision). Robust mechanical sectioning was achieved by an integrated automated vibrating blade microtome. The automated sectioning parameters for the heart tissue were set to at 0.1 mm/s and a 100 μm thickness. The reliability of sectioning was verified by measurements of the hearts surface and 20% overlapping Z-planes before and after sectioning during the whole dataset. The imaging wavelength was 810 nm and tissue and image acquisition parameters: 18000x16000 pixels and 6.80 mm x 6.05 mm (1 pixel = 0.378 μm).

In Figure 1, a subregion of one of the microscopy images is shown, where the myocytes forming the fibers can be distinguished. The nuclei of the myocytes can be seen as low intensity elliptical structures. By visual inspection of the cells, the elongated structures with higher intensity values can be noticed, following the fibers direction. In this section we explore this feature of the image using a method that detects the main direction of the fiber structures, as well as the magnitude associate to the secondary direction. This information provide us with a tensor representation of the cardiac tissue.

2.2 Method

Our goal is to obtain image descriptors that capture the local shape of the underlying structure from the multi-photon microscopy images. This local shape can be represented as a second order tensor, that provides information about the local main orientation and the fiber compactness. Therefore, a feature detection method has to be applied over the image. In different intensity based feature

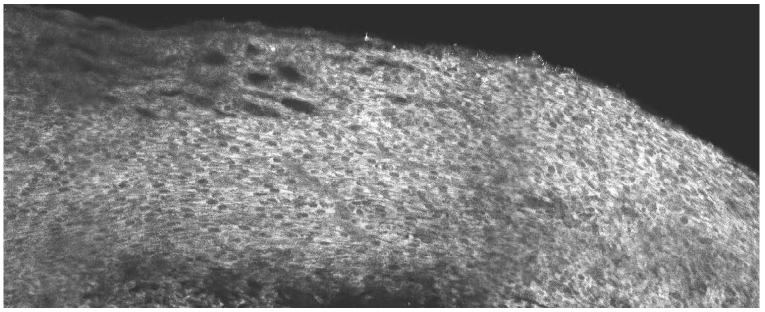

Fig. 1. Subregion of one microscopy image obtained from the heart of a fetal rabbit

detection techniques, variation of intensity contrast in the image can effect dramatically the boundary detection results, especially for low contrast structures. For this reason, the local phase of the image was chosen to avoid this problem. Local phase information is brightness- and contrast-invariant and has been successfully used before to detect local changes in image structures. Therefore, we will compute the local phase information of the image, $\phi_{s,t}$ at a given scale s and orientation t, as in [12]. Given the image at each point $\mathbf{x}$, as $I(\mathbf{x})$, and a pair of quadrature filters $F_{s,t}^{even}$ and $F_{s,t}^{odd}$ at scale s, and orientation t, the local phase is defined as

$$\phi_{s,t}(\mathbf{x}) = atan(u_{s,t}(\mathbf{x})/v_{s,t}(\mathbf{x})),$$

where $u_{s,t}(\mathbf{x})$ and $v_{s,t}(\mathbf{x})$ are the convolutions of the image with the quadrature filters:

$$[u_{s,t}(\mathbf{x}), v_{s,t}(\mathbf{x})] = [I(\mathbf{x}) * F_{s,t}^{even}, I(\mathbf{x}) * F_{s,t}^{odd}].$$

The quadrature filters are log-Gabor filters that have been successfully applied before [13]. To illustrate the local phase result in our particular case, a subset of one image acquired is shown in Figure 2 (a), and its computed local phase $\phi(\mathbf{x})$, averaged over a set of scales and integrated over all directions, Figure 2 (b). In this work all experiments were performed using five scale levels.

Now, the important information of the image can be extracted and processed to estimate the main local directions of the underlying cellular structure. To obtain this information, the results of multi-scale local phase is thresholded using a value θ that keeps the most important features of the image. Typically this will provide us with the elongated structures present in the image as well as some outliers which are very small structures coming from homogeneous regions in the original image. The optimal threshold value is selected based on the best performance of our technique with testing different threshold values. These small regions are removed using image connectivity and a filter with size criteria, see Figure 2 (c). After that, each connected component was analyzed and the main direction $\mathbf{e}_1$, which give us the fiber direction, was obtained. The second direction

$\mathbf{e}_2$ is simply taken as the perpendicular direction to $\mathbf{e}_1$. The ratio $R = M/m$ is also computed, where M and m indicate the maximum elongation along the $\mathbf{e}_1$ and $\mathbf{e}_2$ direction, respectively. With this information we can represent the local shape and the direction of the microstructure of the cardiac tissue.

To represent the results obtained, each connected component can be associated with a tensor located at the centroid of the connected component, with eigenvectors given by the principal directions obtained $\mathbf{e}_1$, $\mathbf{e}_2$ and eigenvalues relation given by the the ratio R, using a fixed major eigenvalue for all the tensors. This sparse tensor field result can be also viewed as a sparse ellipse representation of the cardiac structure, as the one shown in Figure 2 (d). Notice that the ellipses shown here are not supposed to label myocytes. They are a local representation of the tissue structure. These ellipses will point into the fibers direction and they are more elongated when the myocytes are more compactly arranged. Therefore, the way they are shown in the image is a good representation of the microstructure of the tissue, that means, the microfibers direction and their compactness.

As we are interested in the structures providing directional information along the microfibers, two final post-processing steps are performed. The first one is performed to remove tensors with major eigenvector pointing into a very different direction than the majority of components (orientation outliers). Due to image characteristics, structures going in very different fiber directions than the microfibers directions may appear, mainly in regions between cells nuclei.

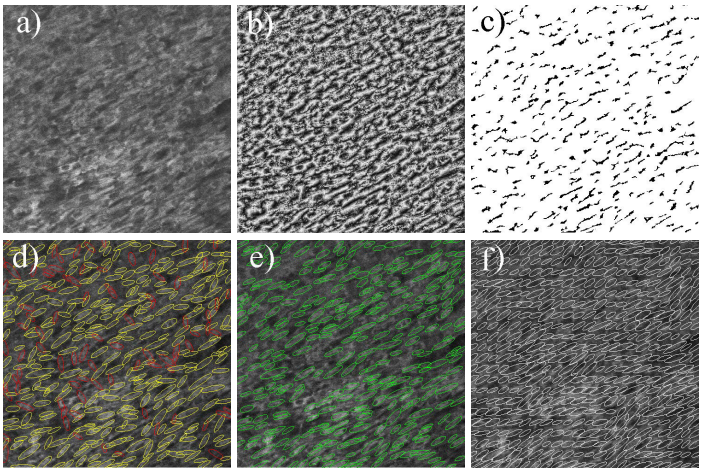

Fig. 2. a) subset of one of the acquired images, $I(\mathbf{x})$; b) local phase obtained from it, $\phi(\mathbf{x})$; c) connected components obtained from the local phase; d) ellipse representation of the underlying cardiac structure (in yellow following the fiber direction, in red the orientation outliers); e) ellipses after gaussian filtering of the orientation; f) ellipses after interpolation

These regions account for a low number of the components obtained, and can be locally detected and removed using a median filter in the orientation values. Once these outliers are removed, a gaussian smoothing is performed over the orientations of the remaining tensors, in order to reduce noise, see Figure 2 (e). Finally, the rest of the tissue can be filled using interpolation. The interpolation used here is a linear interpolation on the orientations and ratio values, and is illustrated in Figure 2 (f).

3 Results

In this section we present some results. First, using digital phantom data to observe, in a controlled image, the behaviour of the direction and the shape of the estimated local image descriptors. Then, results in several real images are presented.

3.1 Phantom Data

The phantom image used in this experiment has been generated using a simple pattern as shown in Figure 3 (a). This image resembles a normal but regular pattern of the myocytes, as observed in the multi-photon microscopy images used. The fibers are generated by following concentric circular trajectories using consecutive ellipsoidal shapes. The image has been blurred with a gaussian filter using a sigma value of 3 in pixel dimensions. Then, gaussian noise was added, with zero mean and different variance values, obtaining images with signal-to-noise ratio (SNR) from 0.02 to 9.8. These images were used to test our method, measuring the average angle difference between the reference phantom and the main direction obtained in our results at each image point. Different threshold values for local phase were tested on an image with SNR of 0.60, obtaining an optimal threshold value of 0.55, based on the performance of our method. The average angle differences for different SNR and thresholds are reported in Table 1. The results of local shapes can be observed in Figure 3 (b), for a SNR of 0.60, where it can be seen that the pattern is recovered using ellipsoidal visualization. This enables us to represent both the orientation and the compactness of the tissue.

We represent the main local directions obtained as a vector field, as well as using paths following the microfibers, represented as streamlines in Figure 3 (c). In order to see how the direction of microfibers is recovered, we compared this result with the true paths used in the phantom creation and shown in Figure 3 (d). It can be noticed that fiber directions are correctly recovered.

A second experiment has been carried out to show how the myocytes compactness can be detected locally. In this case, the results from the same phantom shown above were compared to the results of a similar phantom but with increased distance between fibers and increased thickness of the myocytes. This comparison is presented in Figure 4, where a subregion of the two phantoms and their corresponding ellipsoidal representations of local shape are shown, indicating that both cases have identical orientations but different local shapes.

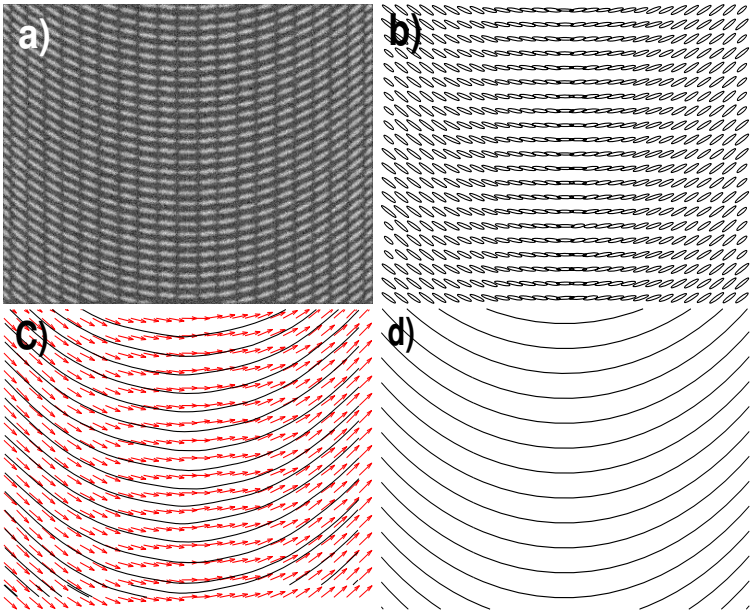

Fig. 3. a) Digital phantom with myocyte pattern similar to multi-photon microscopy imaging; b) local shapes estimated from the image using the proposed method; c) vector field and streamlines representing the path followed by the microfibers; and d) true paths followed by the phantom fibers

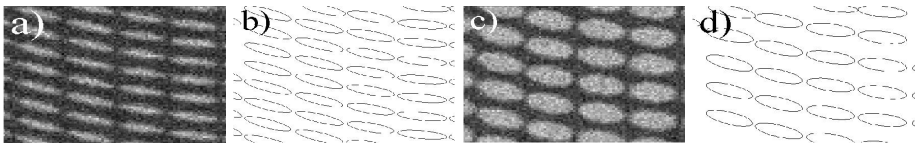

Fig. 4. Comparison between two phantoms, a) and c), presenting different compactness. The results, b) and d), show identical directions but increased size of the local shapes in the secondary direction for the second phantom

3.2 Multi-photon Microscopy Images

The results obtained from microscopy data acquired with the multi-photon microscope aforementioned can be seen in Figure 5, where the first column shows the microscopic images, the second the local shapes detected, the third the interpolated values, and the last column shows the main local orientations of the data as a vector field, $\mathbf{e}_1$, and the streamlines following the microfibers obtained from these local orientations. The streamlines are computed by an integration method over the vector field using points at the borders of the image as starting points.

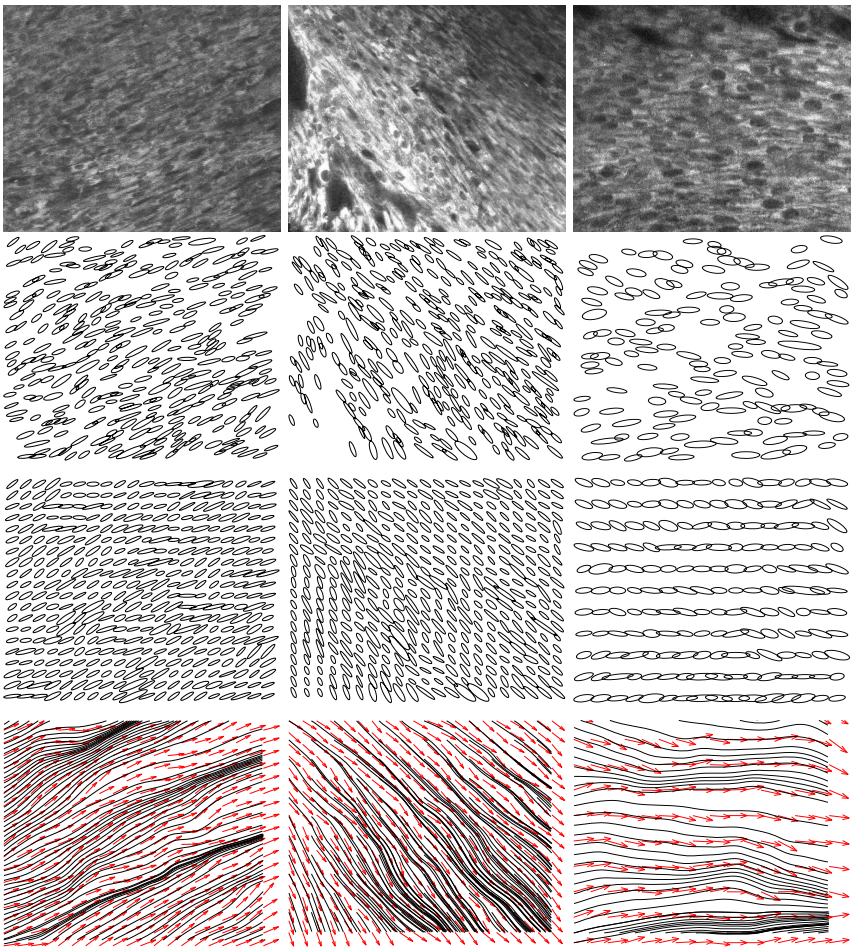

Fig. 5. Multi-photon microscopic images (first row); tensor field shown as ellipses, and obtained with our method (second row); interpolated tensor field (third row); vector field of the main local orientation $\mathbf{e}_1$, and streamlines representing the path followed by the microfibers (fourth row)

Table 1. Average angle difference changes in degrees with respect to different SNR values and threshold values of the local phase, computed in the phantom of Figure 3 (a)

Signal-to-noise ratio	9.80	2.44	1.09	0.60	0.39	0.15	0.03	0.02
Average angle difference	1.47	1.46	1.42	1.46	1.46	1.73	5.10	8.80

Local phase threshold	0.15	0.25	0.35	0.45	0.55	0.65	0.75	0.85
Average angle difference	1.41	1.55	1.50	1.42	1.40	1.43	1.99	19.13

4 Conclusions

We have presented a novel approach that shows a great potential to study the cardiac structure from multi-photon confocal microscopy. The experiments carried out shows a good behaviour of the method, that is able to track correctly the cardiac fibers at microscopic level, and accounts also for their compactness. This work has to be considered as a starting point for a more challenging task that implies extending and applying this methodology to the whole heart using serial sections of the heart to obtain a detailed and realistic model of the cardiac fiber structure. This model will be of great value to validate data coming from other modalities such as DTI or to generate more realistic simulations. Additionally, similar experiments can be also performed to generate detailed fiber models of diseased hearts, applying the same methodology, that can be compared with a control heart model to understand their differences at microscopic level.

Acknowledgment. This study was partially supported by the Subprograma de Proyectos de Investigacin en Salud. Instituto de Salud Carlos III, Spain (FIS - PI11/01709). Special thanks to Dr. Tim Ragan, from Tissue Vision [1], for providing us with the data for this work.

References

1. Bishop, M.J., Plank, G., Burton, R.A.B., Schneider, J.E., Gavaghan, D.J., Grau, V., Kohl, P.: Development of an anatomically detailed MRI-derived rabbit ventricular model and assessment of its impact on simulations of electrophysiological function. American Journal of Physiology. Heart and Circulatory Physiology 298(2), H699–H718 (2010)
2. Punske, B.B., Taccardi, B., Steadman, B., Ershler, P.R., England, A., Valencik, M.L., McDonald, J.A., Litwin, S.E.: Effect of fiber orientation on propagation: electrical mapping of genetically altered mouse hearts. Journal of Electrocardiology 38(4), 40–44 (2005)
3. Weiss, D., Seemann, G., Keller, D., Farina, D., Sachse, F., Dossel, O.: Modeling of heterogeneous electrophysiology in the human heart with respect to ECG genesis. In: Computers in Cardiology, pp. 49–52. IEEE (2007)
4. Billet, F., Sermesant, M., Delingette, H., Ayache, N.: Cardiac motion recovery and boundary conditions estimation by coupling an electromechanical model and cine-MRI data. In: Ayache, N., Delingette, H., Sermesant, M. (eds.) FIMH 2009. LNCS, vol. 5528, pp. 376–385. Springer, Heidelberg (2009)
5. Chang, H.H., Moura, J.M., Wu, Y.L., Sato, K., Ho, C.: Reconstruction of 3d dense cardiac motion from tagged MR sequences. In: IEEE International Symposium on Biomedical Imaging: Nano to Macro, pp. 880–883. IEEE (2004)
6. Arts, T., Prinzen, F.W., Snoeckx, L., Rijcken, J.M., Reneman, R.S.: Adaptation of cardiac structure by mechanical feedback in the environment of the cell: a model study. Biophysical Journal 66(4), 953–961 (1994)
7. Arts, T., Reneman, R.S., Veenstra, P.C.: A model of the mechanics of the left ventricle. Annals of Biomedical Engineering 7(3), 299–318 (1979)

[1] `www.tissuevision.com`

8. Bovendeerd, P., Arts, T., Huyghe, J., Van Campen, D., Reneman, R.: Dependence of local left ventricular wall mechanics on myocardial fiber orientation: a model study. Journal of Biomechanics 25(10), 1129–1140 (1992)
9. Chadwick, R.: Mechanics of the left ventricle. Biophysical Journal 39(3), 279–288 (1982)
10. Streeter, D.D., Spotnitz, H.M., Patel, D.P., Ross, J., Sonnenblick, E.H.: Fiber Orientation in the Canine Left Ventricle during Diastole and Systole. Circulation Research 24(3), 339–347 (1969)
11. Lekadir, K., Ghafaryasl, B., Muñoz-Moreno, E., Butakoff, C., Hoogendoorn, C., Frangi, A.F.: Predictive modeling of cardiac fiber orientation using the knutsson mapping. In: Fichtinger, G., Martel, A., Peters, T. (eds.) MICCAI 2011, Part II. LNCS, vol. 6892, pp. 50–57. Springer, Heidelberg (2011)
12. Kovesi, P.: Image features from phase congruency. Videre: Journal of Computer Vision Research 1(3), 1–26 (1999)
13. Field, D.J., et al.: Relations between the statistics of natural images and the response properties of cortical cells. J. Opt. Soc. Am. A 4(12), 2379–2394 (1987)